International Journal of Minerals, Metallurgy and Materials
Volume 28, Number 12, December 2021, Page 1929
https://doi.org/10.1007/s12613-020-2118-9

Rapid removal of copper impurity from bismuth–copper alloy melts via super-gravity separation

Xiao-chun Wen, Lei Guo, Qi-peng Bao, and Zhan-cheng Guo

State Key Laboratory of Advanced Metallurgy, University of Science and Technology Beijing, Beijing 100083, China
(Received: 26 April 2020; revised: 29 May 2020; accepted: 15 June 2020)

Abstract: A green method of super-gravity separation, which can enhance the filtration process of bismuth and copper phases, was investigated and discussed for the rapid removal of copper impurity from bismuth–copper alloy melts. After separation by the super-gravity field, the bismuth-rich liquid phases were mainly filtered from the alloy melt along the super-gravity direction, whereas most of the fine copper phases were retained in the opposite direction. With optimized conditions of separation temperature at 280°C, gravity coefficient at 450, and separation time at 200 s, the mass proportion of the separated bismuth from the Bi–2wt%Cu and Bi–10wt%Cu alloys respectively reached 96% and 85% , which indicated the minimal loss of bismuth in the residual. Simultaneously, the removal ratio of impurity copper from the Bi–2wt%Cu and Bi–10wt%Cu alloys reached 88% and 98%, respectively. Furthermore, the separation process could be completed rapidly and is environmentally friendly and efficient.

Keywords: rapid removal; copper impurity; bismuth–copper alloys; filtration; super-gravity field

1. Introduction

Bismuth, as a green metal, is gradually replacing toxic metals, such as lead, antimony, and mercury, in the metallurgical and chemical industries [1]. However, various impurity elements, which are the intermediate products obtained from the pyrometallurgical or hydrometallurgical processing of bismuth-containing raw materials, are present in crude bismuth [2]. These impurities will affect the performance of metallic bismuth if they remain unremoved. In general, crude bismuth must be refined through pyro refining and electrorefining. Especially, the first process removes copper impurity by combining liquation and sulfureting methods in the pyro refining process [3]. Nevertheless, the separation of bismuth and copper metals is difficult given their thermodynamic properties [4–5] and is a complicated process due to the required repeated collection of slags and large energy consumption during the liquation process. In addition, the environmental pollution is serious in terms of large quantity of waste emissions and smoke dust produced during the sulfureting process. Currently, several methods, such as crystallization [6], hydrometallurgical process [7], and vacuum distillation [8], have been proposed for the decoppering process; these methods effectively remove impurity copper from the crude bismuth. However, these procedures can hardly meet the energy-saving and clean production requirements due to their high cost, complicated process, and low removal efficiency. Therefore, studies should explore improved and innovative methods of removing impurity copper from the crude bismuth.

Super-gravity technology has attracted considerable attention from metallurgists given its characteristic of enhancing the processes of mass transfer and phase migration. Super-gravity is mainly used in the segregation of precipitated phases from melt mixture [9–10], such as removal of the inclusion phases from metal melts, concentration of valuable resources from molten slags, separation of valuable metals from e-waste. Numerous researchers are devoted to the separation of impurities from metal melts or alloys by super-gravity technology. Li *et al*. [11] reported that the fine Al_2O_3 inclusions in liquid steel can be efficiently separated and removed by super-gravity technology, and the removal ratio of total oxygen content can reach up to 95.6%. Zhao *et al*. [12] studied the enrichment and removal of low-content impurities from Al via solidifying Al with super-gravity technology. Song *et al*. [13] proposed an innovative method for the separation of nonmetallic inclusions from the aluminum melt under a super-gravity field, and the results showed that the

Corresponding authors: Lei Guo Email: leiguo@ustb.edu.cn; Zhan-cheng Guo Email: zcguo@ustb.edu.cn

volume fraction, number density, and average size of inclusions gradually increases in the samples along the direction of super-gravity. Lan *et al*. [14] reported the super-gravity separation of rare earths elements from rare-earth tailings, which are massively stockpiled in Bayan Obo tailings dams; the high-purity rare-earth oxyfluoride, rare-earth ferrate, and britholite phases were obtained. Wang *et al*. [15] studied the recovery of zinc from galvanizing dross with a super-gravity field, and over 79wt% zinc was recovered with a high purity of about 99wt% by the conditions of gravity coefficient (G) ≥ 500, separation time (t) ≥ 180 s, and separation temperature (T) = 510°C. Gao *et al*. [16] proposed the recovery of crown zinc and metallic copper from copper smelter dust via evaporation, condensation, and super-gravity separation, with high purity of 98.57wt% and 99.99wt%, respectively. The enrichment and separation of impurity copper from the Pb–3wt%Cu alloy melt via the super-gravity field was reported by Yang *et al*. [17], and the results showed that the entire impurity copper phase gathers at the upper area of the sample. In addition, Guo *et al*. [18] investigated the removal of tramp elements from 7075 alloys using the super-gravity-aided rheorefining approach; the finely distributed impurity elements, such as Zn, Cu, and Mg, mainly forms as the filtrate, and the time for effective separation of liquid/solid phases can be restricted to 1 min. Super-gravity can also be applied to separate the Fe-bearing and P-bearing phases from steelmaking slag [19], the anosovite crystals [20] and perovskite crystals [21] from molten Ti-bearing slag, and the copper phase and iron-rich phase from copper slag [22]. The above-mentioned applications demonstrate that super-gravity filtration is an effective means for massive-scale separation and removal of impurities from metal melts or alloys. However, limited research investigated the separation of Bi–Cu melt by super-gravity. The Bi–Cu system has the advantages of good fluidity, low viscosity, and low separation temperature compared with the oxide melts for super-gravity treatment. Simultaneously, this system has the characteristics of simple operation, high efficiency, zero wastewater drain, and dust emission.

The removal of impurity copper from Bi–Cu alloy melts was conducted via super-gravity separation. Based on the theoretical analysis of Bi–Cu phase diagram, the effect of G, T, and t on the removal of impurity copper from Bi–Cu alloy melts was investigated, and the corresponding mechanism was further analyzed. Simultaneously, the area fraction and average diameter of impurity copper phases in the filtrated bismuth obtained by super-gravity separation were discussed. The proposal of an innovative approach for refining crude bismuth by super-gravity technology is expected in the future.

2. Experimental

2.1. Apparatus

Fig. 1 shows the diagrammatic sketch of the centrifugal equipment and filtration device used in this study. The equipment was used for the removal of impurity copper from Bi–Cu alloy melts via super-gravity. The super-gravity filtering device is mainly composed of two graphite crucibles which can be tightly matched with equal internal diameter (Fig. 1(a)). A number of pores are dispersed on the bottom of the upper crucible to facilitate filtration. The stainless-steel filter is selected as the filtration medium, and it can prevent the residual copper from migrating down during the filtration process. The centrifugal apparatus mainly includes a heating furnace and a counterweight, which are symmetrical to the two sides of the centrifugal axis (Fig. 1(b)). Especially, the heating furnace consists of a rotating system, a resistance-heating system, thermal insulation material, and cylindrical

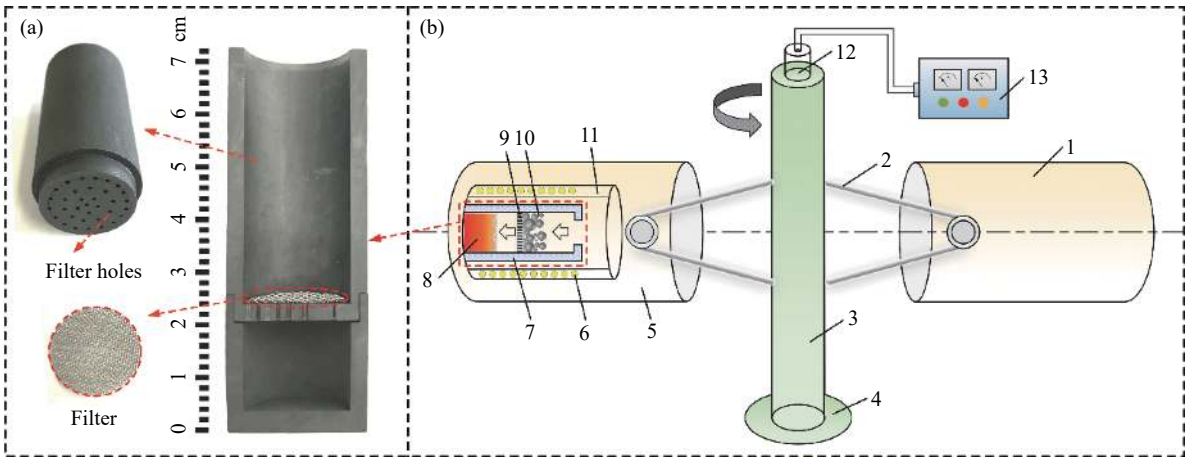

Fig. 1. (a) Separation of the graphite crucible and stainless-steel filter; (b) schematic of the separation equipment: 1—counterweight, 2—centrifugal rotor, 3—centrifugal axis, 4—pedestal, 5—heating furnace, 6—resistance coil, 7—graphite crucible for filtration, 8—filtrated bismuth-rich phase, 9—filter medium of stainless steel, 10—residue impurity copper, 11—cylindrical corundum chamber, 12—conductive slipping, and 13—temperature controller.

corundum chamber (inner diameter: 40 mm; length: 150 mm). The center of gravity and weight of the heating furnace and counterweight should be consistent to ensure the stable operation of the equipment in the centrifugation process. In addition, the temperature was measured by a K-type thermocouple with the maximum permissible error of ±3°C.

In general, the parameter characterization of the magnitude of centrifugal force is defined as the G, as shown in Eq. (1). In this work, the maximum centrifugal force of the separation apparatus can reach $G = 1000$.

$$G = \frac{\sqrt{g^2 + (\omega^2 R)^2}}{g} = \frac{\sqrt{g^2 + (\frac{N^2\pi^2 R}{900})^2}}{g} \quad (1)$$

where ω denotes the angular velocity of the centrifugal apparatus (rad/s), R is the distance from the centrifugal axis to the center of a sample ($R = 0.25$ m), N is the speed of centrifugal force (r/min), g is normal gravity acceleration ($g = 9.8$ m·s^{-2}), and G refers to the gravity coefficient. When the equipment is not started, the centrifugal speed $N = 0$ r/min, and $G = 1$.

2.2. Materials and preparation

In this study, Bi–Cu alloys containing about 2wt% and 10wt% copper were selected as experimental materials. High-purity elemental powders of bismuth (99.999wt%) and copper (99.99wt%) were initially blended in the graphite crucibles, which were then placed in the electric resistance furnace. After heating at 1100°C for 30 min with the protection of high-purity argon atmosphere, the samples were cooled to room temperature for the subsequent super-gravity separation.

2.3. Procedure and analysis

In the separation experiments, the mass of each rod-like specimen was approximately 30 g, and the experimental procedure was mainly as follows. First, the pre-manufactured sample was placed in a graphite filter crucible (Fig. 1(a)). Then, the sample was heated to the target temperature for 25 min to achieve the solid and liquid phase coexisting state. Afterward, the filtration equipment was operated at a desired rotating speed for isothermal separation, after which the centrifugal treatment with a certain filtration time was performed, and the samples were removed from the heating furnace for air cooling. The residual copper and filtered bismuth were obtained from the upper and lower containers of the graphite filter crucible, respectively, and prepared for further analysis.

The lower sample obtained in the super-gravity field was cut longitudinally into two parts along the center axis. One-half was burnished, polished, and investigated by scanning electron microscopy (SEM) with energy-dispersive X-ray spectroscopy (EDS, MLA 250, FEI Quanta, USA) and optical microscopy (Leica DM6000, Germany) to analyze the micro morphology and macro characterization of the filtered bismuth. Moreover, the diameter and area fraction of the impurity copper were characterized by Image-Pro Plus 6.0 software. The other half was studied using inductively coupled plasma optical emission spectrometry (ICP-OES, Optima 7000DV, Perkin Elmer, USA) to investigate the chemical compositions of the filtered bismuth. Moreover, the removal ratio of impurity copper was calculated in detail.

3. Results and discussion

3.1. Theoretical analysis based on the Bi–Cu phase diagram

Fig. 2 depicts the Bi–Cu binary phase diagram which displays the liquid phase and solid solutions of (Cu) and (Bi) based on the status of thermodynamic description [23]. Copper can be continuously crystallized and precipitated in the form of solid phase from the melt during cooling process. The components of the liquid phase change along with the liquidus during the crystallization stage until the final solidification process with the eutectic temperature of ~270°C. In addition, the solid copper phase should automatically move up in the melt theoretically due to the evident density difference between copper and bismuth (8.96×10^3 and 9.8×10^3 kg·m^{-3}, respectively). Moreover, the migration speed of the impurity copper can effectively be strengthened under the super-gravity field in accordance with Stokes's law [24]; thus, the removal of impurity copper from Bi–Cu alloy melts is practicable by super-gravity technology.

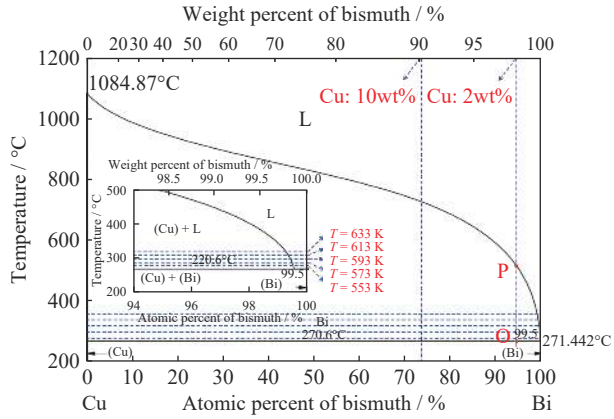

Fig. 2. Bi–Cu binary phase diagram drawn with the ASM Alloy Phase Diagram Database™. Solid phases begin to appear at point P and liquid phases disappear completely at point O during the cooling process.

Therefore, the experimental conditions for this study were designed based on the above theoretical analysis (Table 1). Sixteen trials were conducted in the experiment, and the G were 50, 150, 300, 450, and 600. The t were 50, 100, 150, 200, and 250 s, and the T were 280, 300, 320, 340, and 360°C. In particular, trial 10 and trial 16 under super-gravity and normal-gravity fields, respectively, have been carried out as the contrast experiments.

Table 1. Experimental conditions used in this work

Trial	G	t / s	T / °C	Trial	G	t / s	T / °C
1	50	200	340	9	450	200	340
2	150	200	340	10	450	250	340
3	300	200	340	11	450	200	280
4	450	200	340	12	450	200	300
5	600	200	340	13	450	200	320
6	450	50	340	14	450	200	340
7	450	100	340	15	450	200	360
8	450	150	340	16	1	250	340

The purification ratio of copper and mass proportion of the filtered bismuth were defined to characterize the removing effect of impurity copper from Bi–Cu alloy melts. The content of bismuth in the filtrate was investigated based on ICP-OES results and is represented as $\omega_{\text{Bi-filtered}}$.

The removal ratio of impurity copper (γ_{Cu}) was calculated by Eq. (2):

$$\gamma_{\text{Cu}} = \frac{\omega_{\text{Cu-raw}} - \omega_{\text{Cu-filtered}}}{\omega_{\text{Cu-raw}}} \times 100\% \quad (2)$$

where $\omega_{\text{Cu-raw}}$ denotes the copper content (wt%) in the raw materials, and $\omega_{\text{Cu-filtered}}$ indicates the copper content (wt%) in the filtered bismuth after super-gravity separation.

The mass proportion of filtered bismuth ($\beta_{\text{Bi-rich}}$) was defined via Eq. (3):

$$\beta_{\text{Bi-rich}} = \frac{m_{\text{filtered}}}{m_{\text{residue}} + m_{\text{filtered}}} \times 100\% = \frac{m_{\text{filtered}}}{m_{\text{raw}}} \times 100\% \quad (3)$$

where m_{filtered} denotes the quality of the filtered bismuth that was mainly presented in the lower crucible, m_{residue} represents the quality of residual copper that remained in the opposite direction due to the interception of the stainless-steel filter, and m_{raw} refers to the mass of Bi–Cu alloy melts.

The theoretical $\beta_{\text{Bi-rich}}$ was calculated based on the lever rule of Bi–Cu phase diagram. Simultaneously, the content of Bi in the bismuth-rich phase was obtained, and the theoretical γ_{Cu} was calculated (Table 2). The γ_{Cu} gradually decreases with the increase in the T, whereas $\beta_{\text{Bi-rich}}$ for the Bi–2wt%Cu alloy and Bi–10wt%Cu alloy is stable at ~98% and ~90%, respectively. These findings are caused by the content of the liquid phase close to the side of Bi (Fig. 2). The above calculations have significant theoretical guidance to the subsequent separation experiments.

Table 2. Theoretical analysis based on the Bi–Cu phase diagram

T / °C	Bi–2wt%Cu alloy			Bi–10wt%Cu alloy		
	$\beta_{\text{Bi-rich}}$ / %	$\omega_{\text{Bi-filtered}}$ / wt%	γ_{Cu} / %	$\beta_{\text{Bi-rich}}$ / %	$\omega_{\text{Bi-filtered}}$ / wt%	γ_{Cu} / %
280	98.20	99.86	93.00	90.20	99.86	98.60
300	98.30	99.82	91.00	90.30	99.82	98.20
320	98.35	99.80	90.00	90.35	99.80	98.00
340	98.40	99.73	86.50	90.40	99.73	97.30
360	98.45	99.68	84.00	90.45	99.68	96.80

3.2. Macro- and micro-characterization of the samples

The alloys of Bi–2wt%Cu and Bi–10wt%Cu were used as raw materials for the separation experiments. Fig. 3 illustrates the microstructure of filtered samples obtained by normal-gravity. The light and dark areas mainly denote the bismuth phase and impurity copper phase, respectively. In addition, copper phases presents an irregular and rhombic shape and a polygonal shape in the Bi–2wt%Cu alloy and the Bi–10wt%Cu alloy, respectively. Moreover, the impurity copper is dispersed in the bismuth matrix and is inappropriately removed from Bi–Cu alloy melts by floating up spontaneously under the normal-gravity field.

Fig. 4 describes the macro morphological features of the samples attained after super-gravity filtration by the conditions of T = 340°C, t = 250 s, and G = 450. The alloy materials have multiple colors in terms of the special physicochemical properties of bismuth crystals (Figs. 4(a) and 4(d)). Additionally, the liquid bismuth-rich phases are mainly filtered into the lower crucible, whereas most of the fine impurity copper remains in the opposite direction due to the interception of the stainless-steel filter. Especially, the residual copper is easily crushed into pieces (Figs. 4(c) and 4(f)).

Fig. 5 shows the microcosmic structure of the filtered samples attained via super-gravity separation for the Bi–10wt%Cu alloy. The lower sample is the filtrate, and the upper sample is the residual. Nubble bismuth crystals are found in the residual, and several dendrite copper crystals are sparsely presented in the filtered bismuth phase as depicted in Figs. 5(c) and 5(f), respectively. Moreover, the filtered bismuth occupies a large proportion of the filtered samples, which demonstrates the minimal loss of bismuth in the residual.

3.3. Removal of impurity copper from Bi–Cu alloy melts by super-gravity

In this study, Bi–Cu alloy melts were purified under a super-gravity field with different conditions, and the influence of G, T, and t on the removal of impurity copper from Bi–Cu alloy melts were studied.

3.3.1. Effect of gravity coefficient

In this study, the G during the filtration processes were 50,

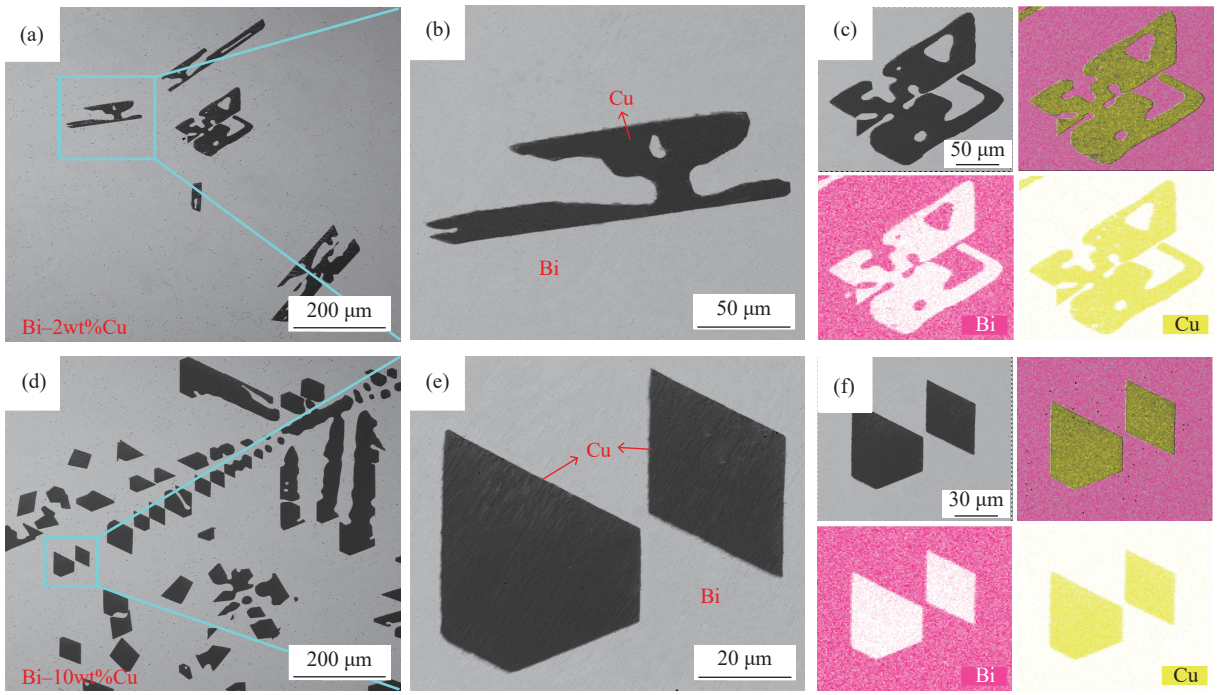

Fig. 3. SEM images of the filtered samples attained by normal-gravity with the conditions of T = 340°C, t = 0 s, and G = 1: (a) micro-characterization of the Bi–2wt%Cu alloy; (b) magnified view of the area indicated in image (a); (c) EDS mapping results of the Bi–2wt%Cu alloy; (d) microstructure of the Bi–10wt%Cu alloy; (e) magnified view of the area indicated in image (d); (f) EDS mapping results of the Bi–10wt%Cu alloy.

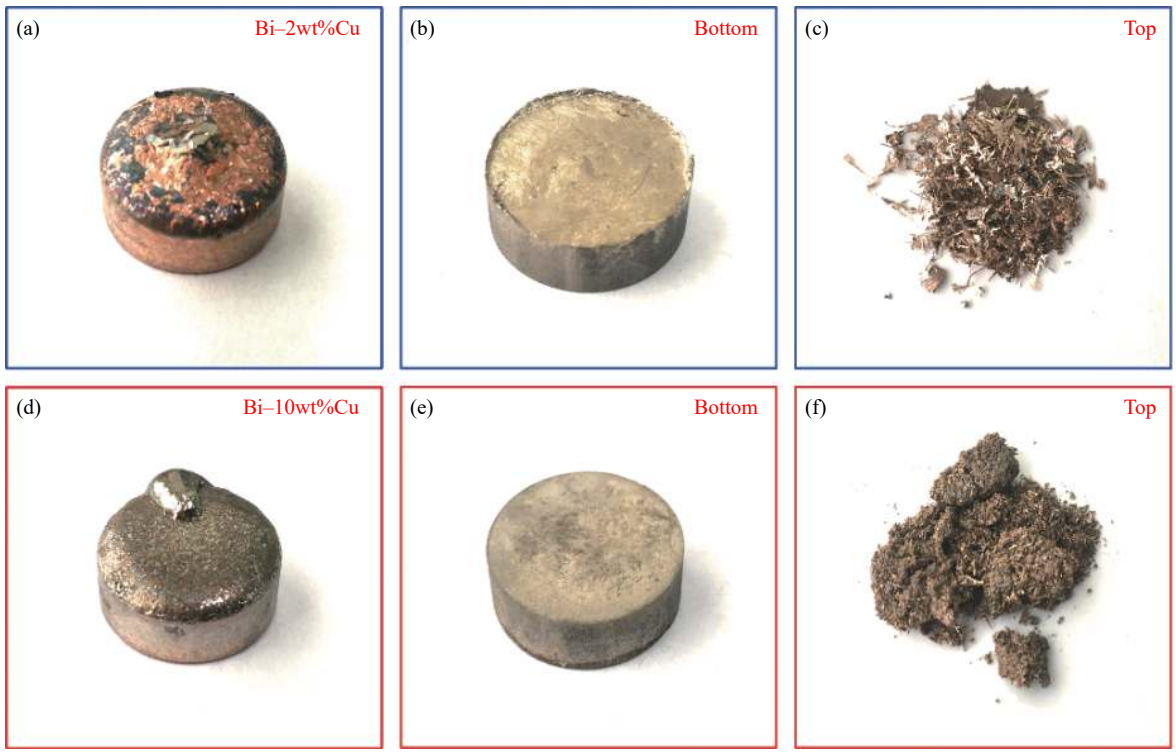

Fig. 4. Macro-morphology of the samples obtained after super-gravity filtration under the conditions of T = 340°C, t = 250 s, and G = 450: (a) Bi–2wt%Cu alloy; (b) filtered bismuth from Bi–2wt%Cu alloy; (c) residual copper phase from Bi–2wt%Cu alloy; (d) Bi–10wt%Cu alloy; (e) filtered bismuth from Bi–10wt%Cu alloy; (f) residual copper phase from Bi–10wt%Cu alloy.

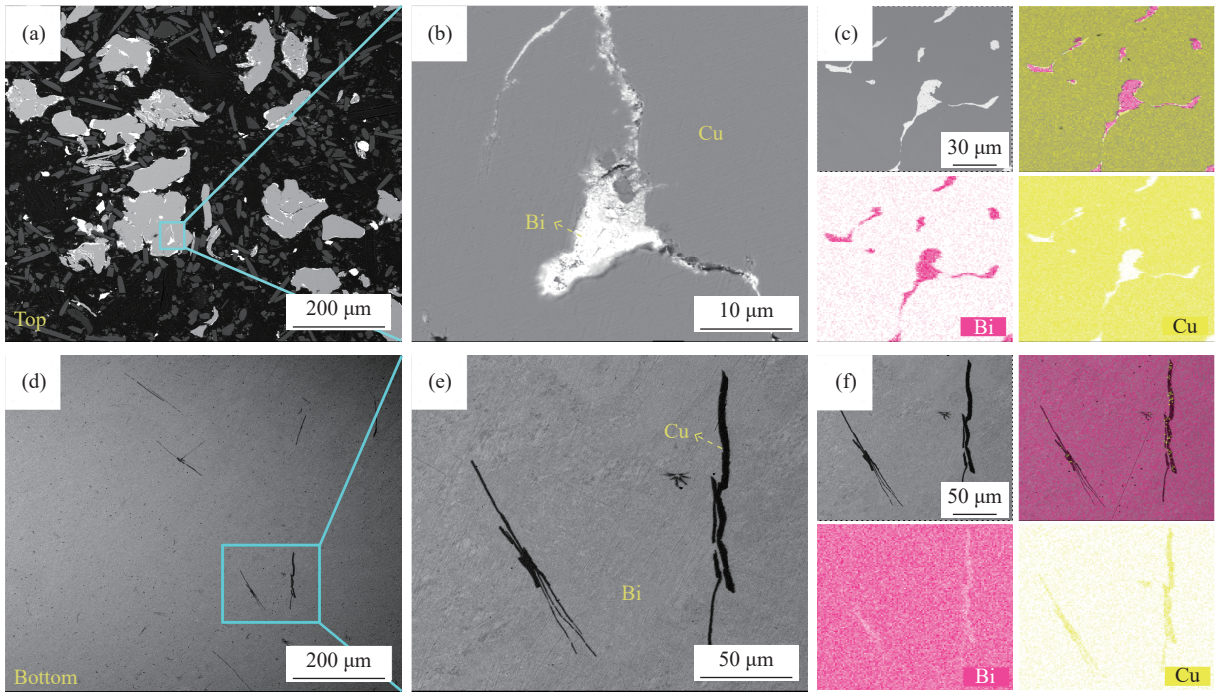

Fig. 5. SEM images of the filtered samples attained after super-gravity filtration under conditions of T = 340°C, t = 250 s, and G = 450 for the Bi–10wt%Cu alloy: (a) SEM image of the residual copper phase; (b) enlarged the area shown in image (a); (c) EDS mapping results of the residual copper phase; (d) SEM image of the filtered bismuth phase; (e) enlarged the area shown in image (d); (f) EDS mapping results of the filtered bismuth phase.

150, 300, 450, and 600, corresponding to the centrifugal speeds of 423, 733, 1036, 1269, and 1465 r/min, respectively. Fig. 6 shows the effect of G on the removal efficiencies of impurity copper from Bi–Cu alloy melts at t = 200 s and T = 340°C. The $\beta_{\text{Bi-rich}}$ and γ_{Cu} notably improve with the increase in G as a result of the filtration of additional bismuth phases into the lower crucible. With the enhancement of G from 50 to 600, the $\beta_{\text{Bi-rich}}$ of the Bi–2wt%Cu and Bi–10wt%Cu alloys increases quickly up to 97% and 87%, respectively. In addition, γ_{Cu} reachs more than 82% and 95% when $G \geq 450$, respectively. Therefore, super-gravity can effectively remove the impurity copper from Bi–Cu alloy melts when the separation condition is $G \geq 450$.

Fig. 7 shows the microcosmic structures of the filtered bismuth attained after super-gravity filtration for the Bi–2wt%Cu alloy with different G at T = 340°C and t = 200 s. The experimental results show that the dendrite copper crystals decrease rapidly in the bismuth matrix with the increase in G, and several copper phases are present in the filtered bismuth when $G \geq 450$.

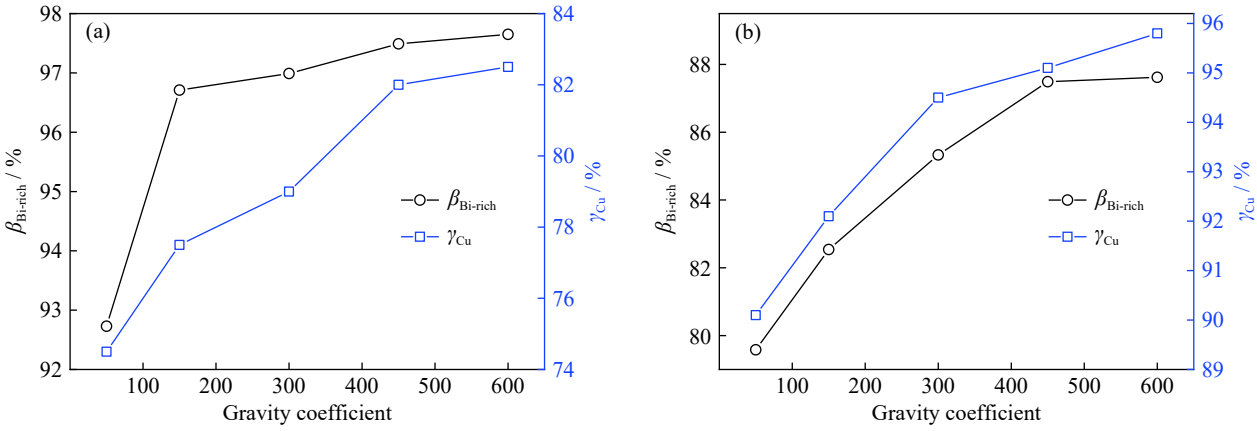

Fig. 6. Effect of G on the removal efficiencies of the impurity copper from different Bi–Cu alloys at T = 340°C, and t = 200 s: (a) Bi–2wt%Cu alloy; (b) Bi–10wt%Cu alloy.

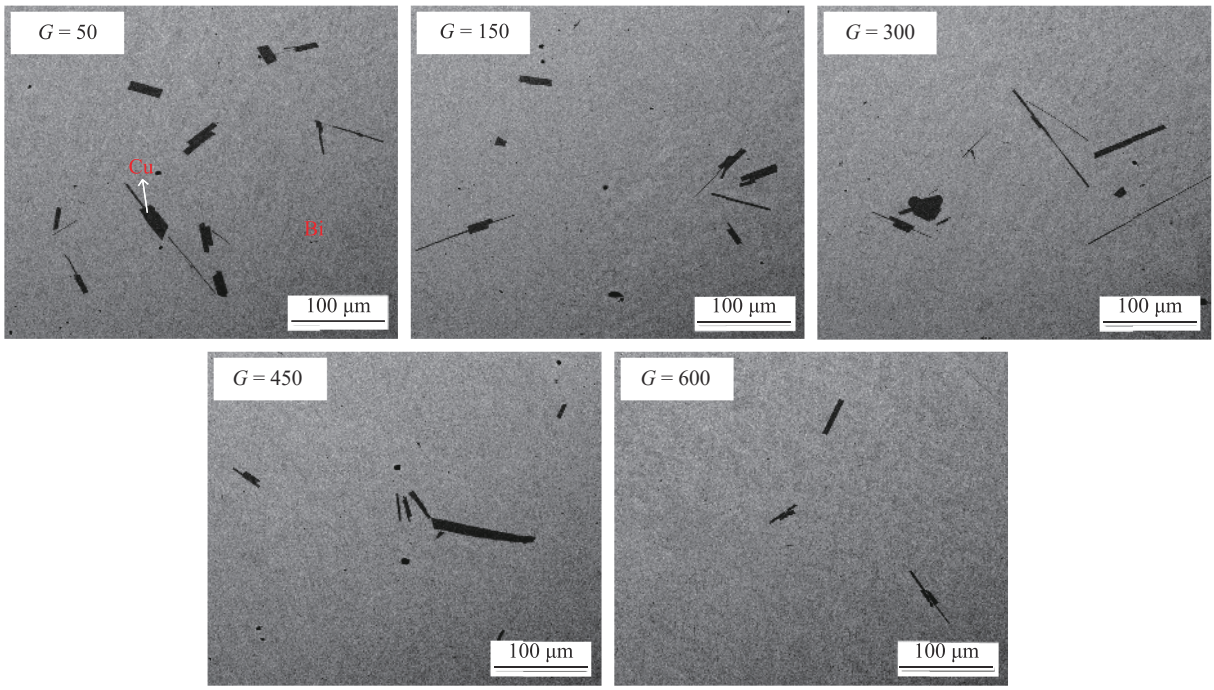

Fig. 7. Microcosmic structure of the filtered bismuth phase attained after super-gravity filtration for the Bi–2wt%Cu alloy by different *G* at *T* = 340°C and *t* = 200 s.

3.3.2. Effect of separation time

Fig. 8 shows the influence of various *t* on the removal efficiencies of impurity copper from Bi–Cu alloy melts at *T* = 340°C and *G* = 450. The $\beta_{\text{Bi-rich}}$ of Bi–2wt%Cu alloy increases steadily from 91% to 97%, and similarly, the $\beta_{\text{Bi-rich}}$ of Bi–10wt%Cu alloy increases gradually from 82% to 87% with increasing *t* from 50 to 250 s. Additionally, the γ_{Cu} of Bi–2wt%Cu and Bi–10wt%Cu alloys approximately stable at 80% and 95%, respectively.

Fig. 9 displays the microscopic images of the separated bismuth attained via super-gravity separation for the Bi–2wt%Cu alloy by various *t* at *T* = 340°C and *G* = 450. Fine impurity copper phases are dispersed in the bismuth melt, and the amount of impurity copper gradually decreases with the increase in *t*. However, when the *t* is greater than 200 s, the content of impurity copper is stable, which indicates that the separation process can be completed in a relatively short time.

3.3.3. Effect of separation temperature

The *T* is an important operating parameter in the experiment. Fig. 10 shows the influence of *T* on the removal efficiencies of impurity copper from Bi–Cu alloy melts at *t* = 200 s and *G* = 450. The γ_{Cu} of Bi–2wt%Cu and Bi–10wt%Cu alloy melts decreases gradually from 88% and 98% to 78% and 94%, respectively when the *T* raises from 280 to 360°C. However, the change of $\beta_{\text{Bi-rich}}$ is not more than 2% when *T*

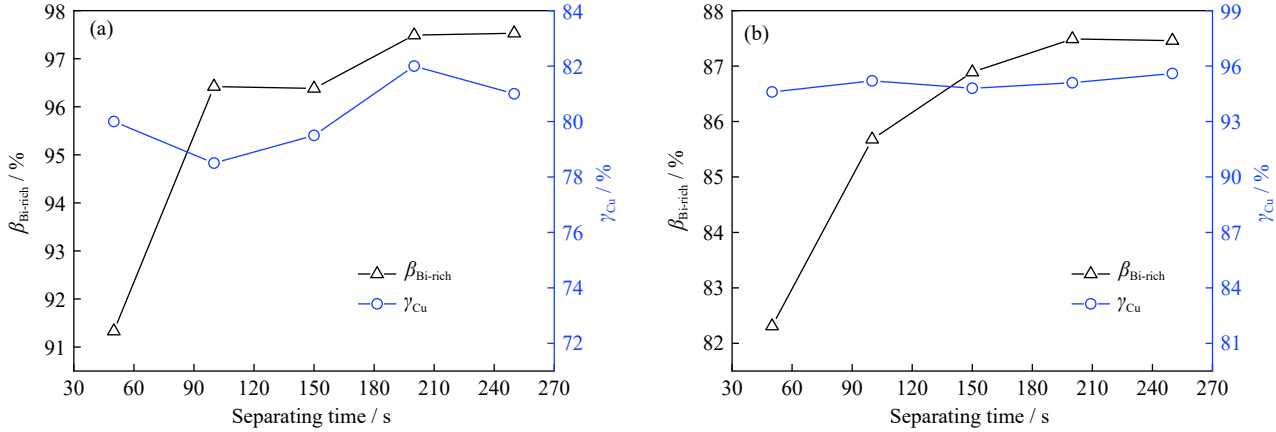

Fig. 8. Effect of various *t* on the removal efficiencies of impurity copper from different Bi–Cu alloy melts at *T* = 340°C, and *G* = 450: (a) Bi–2wt%Cu alloy; (b) Bi–10wt%Cu alloy.

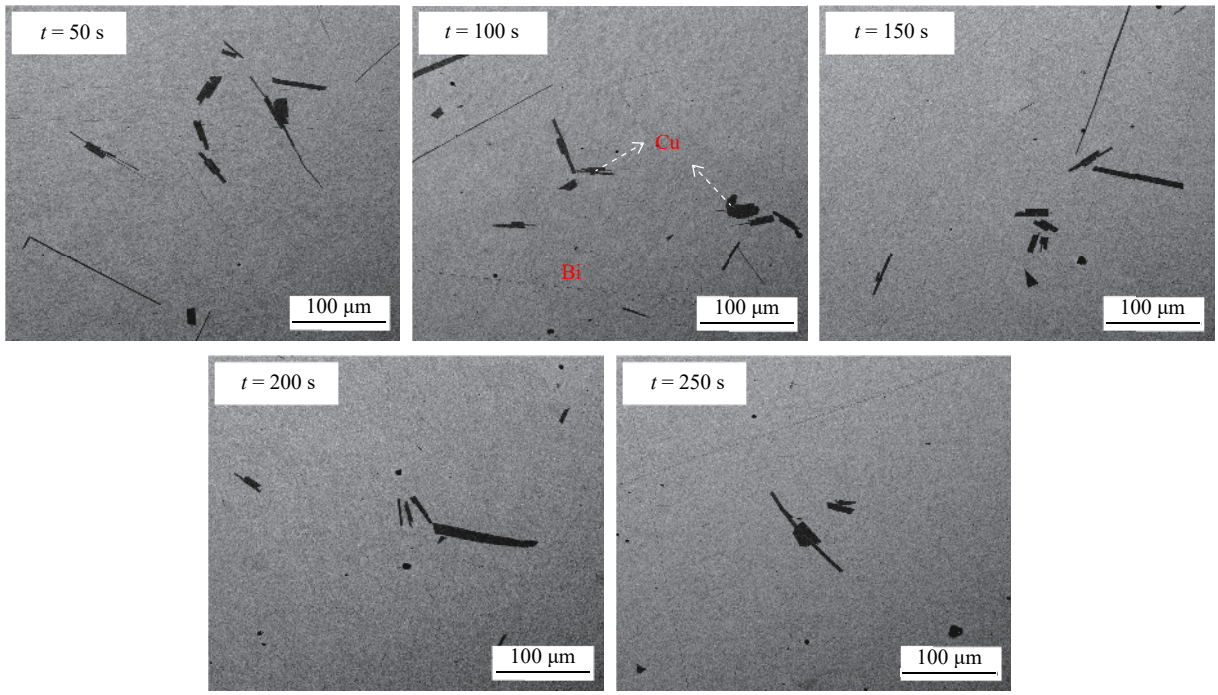

Fig. 9. Microscopic images of the filtered bismuth phase attained via super-gravity separation for the Bi–2wt%Cu alloy by various *t* at *T* = 340°C, and *G* = 450.

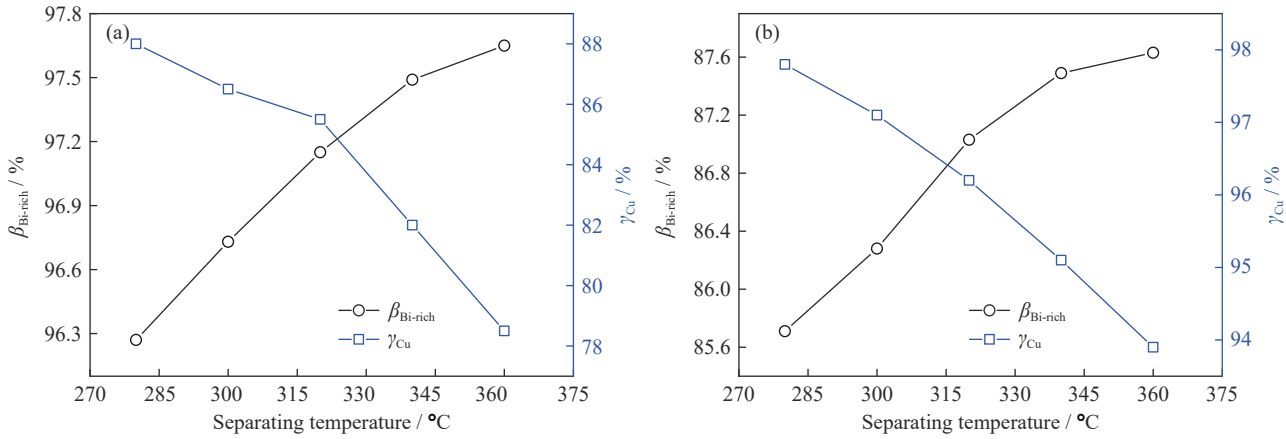

Fig. 10. Effect of various *T* on the removal efficiencies of impurity copper from different Bi–Cu alloy melts at *t* = 200 s, and *G* = 450: (a) Bi–2wt%Cu alloy; (b) Bi–10wt%Cu alloy.

increases from 280 to 360°C and them all exceed approximately 96% and 85% for Bi–2wt%Cu and Bi–10wt%Cu alloy melt, respectively, which exhibits no noticeable improvement regardless of the further increase in *T*. Additionally, the results agree well with the regularities of the Bi–Cu phase diagram. Thus, the experimental data indicate that *T* = 280°C is a suitable operating temperature for the removal of impurity copper from Bi–Cu alloy melts via super-gravity separation.

Fig. 11 displays the microcosmic structures of the filtered bismuth attained after super-gravity filtration of the Bi–2wt%Cu alloy melt under various *T* at *t* = 200 s and *G* = 450. The dark dendrite and gray phases mainly consist of the impurity copper and bismuth matrix, respectively. Furthermore, fine copper phases are dispersed in the filtered bismuth phase, and they increase evidently with the increase in *T*.

Fig. 12 shows the area fraction and average diameter of impurity copper phases in the filtered bismuth attained after super-gravity filtration with optimal conditions of *t* = 200 s, *G* = 450, and *T* = 280°C. The fraction of impurity copper phase with the area of 22.5 μm^2 is about 60%, simultaneously, the diameter of copper particles is mainly between 3 and 13 μm, which indicates that only fine copper phases are existed in the bismuth matrix and are smaller than the size of impurity copper before separation. To further reduce the remaining fine copper impurities in the filtered bismuth, the

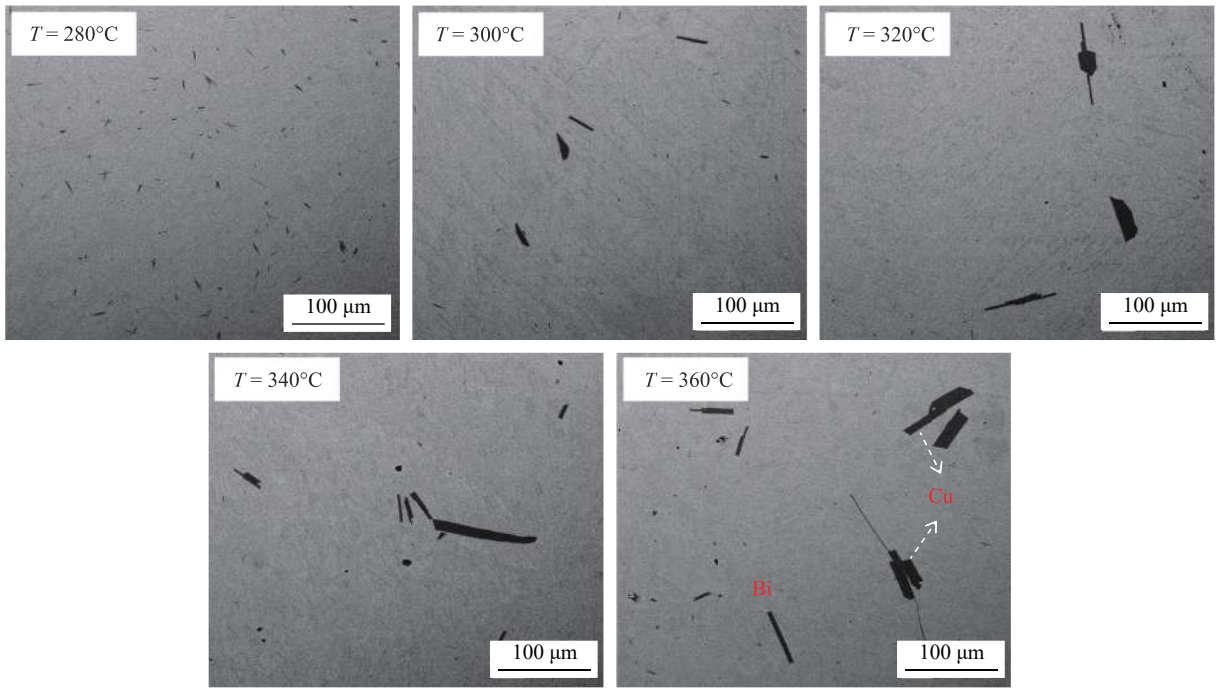

Fig. 11. Microcosmic structure of the filtered bismuth phase attained via super-gravity separation for the Bi–2wt%Cu alloy by different T at t = 200 s, and G = 450.

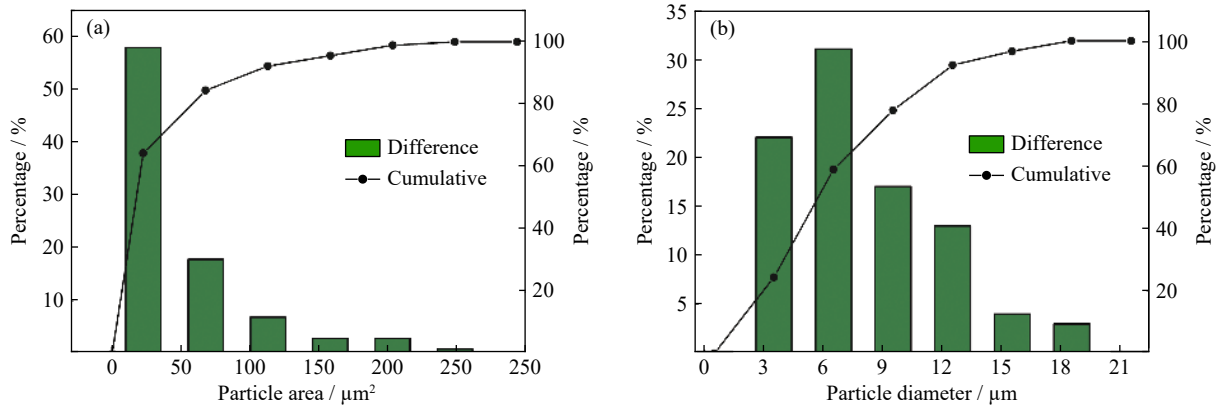

Fig. 12. Area fraction (a) and average size (b) of impurity copper in the filtered bismuth obtained via super-gravity separation at t = 200 s, G = 450, and T = 280°C.

separation conditions like filter medium should be improved.

3.4. Mechanism of removal of impurity copper from Bi–Cu alloys via super-gravity

Fig. 13 shows the mechanism of removal of impurity copper from Bi–Cu alloy melts under the super-gravity field and the migration behavior of metallic copper and bismuth. The results show that the impurity copper is gradually precipitated from the melt in the form of solid phase and is dispersed in the bismuth matrix when the Bi–Cu melt is heated to a specified temperature (Fig. 13(a)). In particular, most of the liquid bismuth-rich phases pass through the stainless-steel filter and are separated to the lower part of the crucible in the direction of super-gravity (Fig. 13(b)), whereas fine copper phases are intercepted at the upper part of the crucible (Fig. 13(c)). Consequently, the removal of impurity copper from Bi–Cu alloy melts can be strengthened in the super-gravity field, and the filtration process has the characteristics of rapidity, environmental friendliness, and efficiency.

4. Conclusions

In this work, the removal of impurity copper from Bi–Cu alloy melts with different G, T, and t was investigated. The main conclusions are as follows.

(1) Theoretical calculation of $\beta_{\text{Bi-rich}}$ and γ_{Cu} was studied in

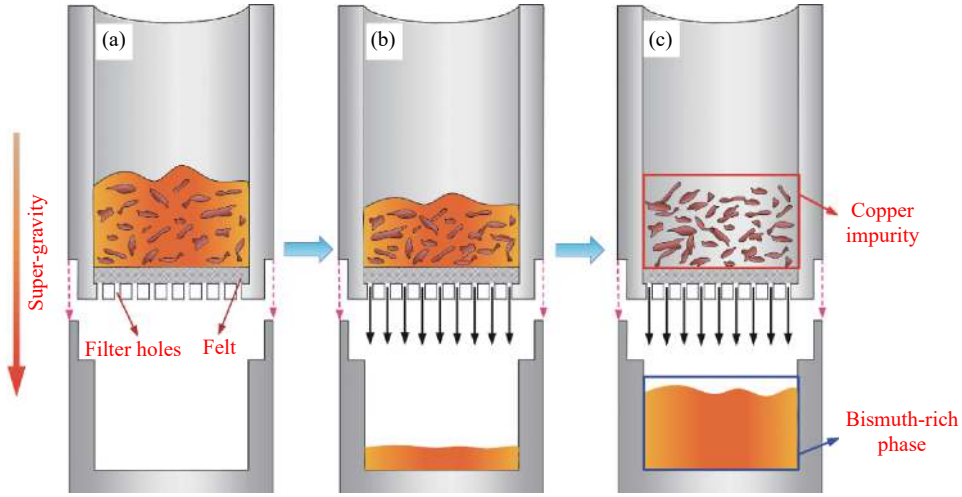

Fig. 13. Mechanism of removal of the impurity copper from Bi–Cu alloy melts under the super-gravity field: (a) the state before separation; (b) the state during separation; (c) the state after separation.

accordance with the lever rule of the Bi–Cu phase diagram; which was agreed well with regularities of the results of separation experiments.

(2) The effect of super-gravity on the removal of impurity copper from Bi–Cu alloy melts was studied in detail. With optimized conditions of T = 280°C, G = 450, and t = 200 s, the $\beta_{\text{Bi-rich}}$ of Bi–2wt%Cu and Bi–10wt%Cu alloy melts reached 96% and 85%, respectively. Simultaneously, γ_{Cu} reached 88% and 98%, respectively.

(3) The removal mechanism of impurity copper revealed that the separation process can be completed in rapid, environment-friendly, and efficient manner.

Acknowledgements

This work was financially supported by the National Natural Science Foundation of China (No. 51804030), and the project of State Key Laboratory of Advanced Metallurgy, China (41618024).

References

[1] F.K. Ojebuoboh, Bismuth—Production, properties, and applications, *JOM*, 44(1992), No. 4, p. 46.

[2] Y.L. He, R.D. Xu, S.W. He, H.S. Chen, K. Li, Y. Zhu, and Q.F. Shen, Alkaline pressure oxidative leaching of bismuth-rich and arsenic-rich lead anode slime, *Int. J. Miner. Metall. Mater.*, 26(2019), No. 6, p. 689.

[3] L.G. Wang, *Metallurgy of Bismuth*, Metallurgical Industry Press, Beijing, 1986, p. 99.

[4] L.S. Chang, E. Rabkin, B.B. Straumal, B. Baretzky, and W. Gust, Thermodynamic aspects of the grain boundary segregation in Cu(Bi) alloys, *Acta Mater.*, 47(1999), No. 15-16, p. 4041.

[5] O. Akinlade, R.N. Singh, and F. Sommer, Thermodynamic investigation of viscosity in Cu–Bi and Bi–Zn liquid alloys, *J. Alloys Compd.*, 267(1998), No. 1-2, p. 195.

[6] W.Z. Guo, *Study on Crystallization Refining of Crude Bismuth* [Dissertation], Central South University, Changsha, 2014, p. 13.

[7] Y. Chen, T. Liao, G.B. Li, B.Z. Chen, and X.C. Shi, Recovery of bismuth and arsenic from copper smelter flue dusts after copper and zinc extraction, *Miner. Eng.*, 39(2012), p. 23.

[8] Y.N. Dai and B. Yang, *Vacuum Metallurgy of Non-ferrous Metals*, Metallurgical Industry Press, Beijing, 2009, p. 128.

[9] J.T. Gao, L. Guo, Y.W. Zhong, H.R. Ren, and Z.C. Guo, Removal of phosphorus-rich phase from high-phosphorous iron ore by melt separation at 1573 K in a super-gravity field, *Int. J. Miner. Metall. Mater.*, 23(2016), No. 7, p. 743.

[10] L. Meng, Z. Wang, Y.W. Zhong, K.Y. Chen, and Z.C. Guo, Supergravity separation of Pb and Sn from waste printed circuit boards at different temperatures, *Int. J. Miner. Metall. Mater.*, 25(2018), No. 2, p. 173.

[11] C. Li, J.T. Gao, Z. Wang, and Z.C. Guo, Separation of fine Al_2O_3 inclusion from liquid steel with super gravity, *Metall. Mater. Trans. B*, 48(2017), No. 2, p. 900.

[12] L.X. Zhao, Z.C. Guo, Z. Wang, and M.Y. Wang, Removal of low-content impurities from Al by super-gravity, *Metall. Mater. Trans. B*, 41(2010), No. 3, p. 505.

[13] G.Y. Song, B. Song, Y.H. Yang, Z.B. Yang, and W.B. Xin, Separating behavior of nonmetallic inclusions in molten aluminum under super-gravity field, *Metall. Mater. Trans. B*, 46(2015), No. 5, p. 2190.

[14] X. Lan, J.T. Gao, Y. Li, and Z.C. Guo, A green method of respectively recovering rare earths (Ce, La, Pr, Nd) from rare-earth tailings under super-gravity, *J. Hazard. Mater.*, 367(2019), p. 473.

[15] Z. Wang, J.T. Gao, A.J. Shi, L. Meng, and Z.C. Guo, Recovery of zinc from galvanizing dross by a method of super-gravity separation, *J. Alloys Compd.*, 735(2018), p. 1997.

[16] J.T. Gao, Z.L. Huang, Z.W. Wang, and Z.C. Guo, Recovery of crown zinc and metallic copper from copper smelter dust by evaporation, condensation and super-gravity separation, *Sep. Purif. Technol.*, 231(2020), art. No. 115925.

[17] Y.H. Yang, B. Song, G.Y. Song, Z.B. Yang, and W.B. Xin, Enriching and separating primary copper impurity from Pb-3 mass pct Cu melt by super-gravity technology, *Metall. Mater. Trans. B*, 47(2016), No. 5, p. 2714.

[18] L. Guo, X.C. Wen, Q.P. Bao, and Z.C. Guo, Removal of tramp elements within 7075 alloy by super-gravity aided rheorefining method, *Metals*, 8(2018), No. 9, art. No. 701.

[19] C. Li, J.T. Gao, Z. Wang, H.R. Ren, and Z.C. Guo, Separation of Fe-bearing and P-bearing phase from the steelmaking slag by super gravity, *ISIJ Int.*, 57(2017), No. 4, p. 767.

[20] Y. Lu, J.T. Gao, F.Q. Wang, and Z.C. Guo, Separation of anosovite from modified titanium-bearing slag melt in a reducing atmosphere by supergravity, *Metall. Mater. Trans. B*, 48(2017), No. 2, p. 749.

[21] J.T. Gao, Y.W. Zhong, and Z.C. Guo, Selective precipitation and concentrating of perovskite crystals from titanium-bearing slag melt in supergravity field, *Metall. Mater. Trans. B*, 47(2016), No. 4, p. 2459.

[22] X. Lan, J.T. Gao, Z.L. Huang, and Z.C. Guo, Rapid separation of copper phase and iron-rich phase from copper slag at low temperature in a super-gravity field, *Metall. Mater. Trans. B*, 49(2018), No. 3, p. 1165.

[23] O. Teppo, J. Niemelä and P. Taskinen, An assessment of the thermodynamic properties and phase diagram of the system Bi-Cu, *Thermochim. Acta*, 173(1990), p. 137.

[24] Y. Watanabe, Y. Inaguma, H. Sato, and E. Miura-Fujiwara, A novel fabrication method for functionally graded materials under centrifugal force: The centrifugal mixed-powder method, *Materials*, 2(2009), No. 4, p. 2510.